View metadata, citation and similar papers at core.ac.uk

brought to you by CORE

provided by Elsevier - Publisher Connector

Cell, Vol. 97, 349–360, April 30, 1999, Copyright ©1999 by Cell Press

# Crystal Structure of Human Cytosolic Phospholipase $A_2$ Reveals a Novel Topology and Catalytic Mechanism

**Andréa Dessen,* Jin Tang, Holly Schmidt, Mark Stahl, James D. Clark, Jasbir Seehra, and William S. Somers***
Biochemistry
Wyeth Research
87 Cambridge Park Drive
Cambridge, Massachusetts 02140

## Summary

**Cytosolic phospholipase $A_2$ initiates the biosynthesis of prostaglandins, leukotrienes, and platelet-activating factor (PAF), mediators of the pathophysiology of asthma and arthritis. Here, we report the X-ray crystal structure of human cPLA$_2$ at 2.5 Å. cPLA$_2$ consists of an N-terminal calcium-dependent lipid-binding/C2 domain and a catalytic unit whose topology is distinct from that of other lipases. An unusual Ser-Asp dyad located in a deep cleft at the center of a predominantly hydrophobic funnel selectively cleaves arachidonyl phospholipids. The structure reveals a flexible lid that must move to allow substrate access to the active site, thus explaining the interfacial activation of this important lipase.**

## Introduction

Leukotrienes and prostaglandins are lipid mediators important in asthma, arthritis, and other inflammatory diseases. Leukotrienes cause airway obstruction in asthmatics through bronchoconstriction, increased mucus secretion, and chemoattraction of inflammatory cells; prostaglandins potentiate pain and edema associated with arthritis (O'Byrne, 1997; Simon et al., 1998). Cytosolic phospholipase $A_2$ (cPLA$_2$) cleaves phospholipid membranes to release arachidonic acid, which in turn is metabolized to prostaglandins by the cyclooxygenase pathway and to leukotrienes by the 5-lipoxygenase pathway. Concomitant with the release of arachidonate, lyso-platelet-activating factor (lyso-PAF) is formed, which can then be acetylated to generate PAF, a molecule also implicated in the pathophysiology of asthma and arthritis (Venable et al., 1993; Tjoelker et al., 1995).

Although cPLA$_2$ is a member of a diverse superfamily of phospholipase $A_2$ enzymes (Dennis, 1997), numerous pieces of evidence have supported its central role in lipid mediator biosynthesis: cPLA$_2$ is the only enzyme that is highly selective for phospholipids containing arachidonic acid in the *sn*-2 position (Clark et al., 1991, 1995; Hanel and Gelb, 1993); activation of cPLA$_2$ or its increased expression has been linked with increased leukotriene and prostaglandin synthesis (Lin et al., 1992a, 1992b, 1993); and following activation, cPLA$_2$ translocates to the nuclear membrane, where it is colocalized with the cyclooxygenase and lipoxygenase that metabolize arachidonate to prostaglandins and leukotrienes (Glover et al., 1995; Schievella et al., 1995). Although these data are compelling, the most definitive evidence for the central role of cPLA$_2$ in eicosanoid and PAF production came from mice made deficient in cPLA$_2$ through homologous recombination (Bonventre et al., 1997; Uozumi et al., 1997). Peritoneal macrophages derived from these animals failed to make leukotrienes, prostaglandins, or PAF. The cPLA$_2$-deficient mice have also been informative of the role of cPLA$_2$ in disease, since these animals are resistant to bronchial hyperreactivity in an anaphylaxis model used to mimic asthma (Uozumi et al., 1997). Thus, despite the size of the phospholipase $A_2$ superfamily, cPLA$_2$ is essential for prostaglandin, leukotriene, and PAF production.

Maximal cPLA$_2$ activation requires sustained phosphorylation and mobilization of intracellular calcium (Lin et al., 1993; Qiu et al., 1998). Calcium activation is mediated by an N-terminal $Ca^{2+}$-dependent lipid-binding (CaLB) domain that colocalizes the catalytic domain with its membrane substrate (Nalefski et al., 1994). The structure of the CaLB domain has been solved (Perisic et al., 1998; Xu et al., 1998), and it is a member of the C2 family; hence, we will use the C2 nomenclature. Extracellular ligands that activate cPLA$_2$ cause the phosphorylation of the catalytic domain on serines 505 and 727 (Lin et al., 1993; Leslie, 1997), two residues that are conserved across all species and are phosphorylated in multiple cell types (de Carvalho et al., 1996; Börsch-Haubold et al., 1998). Although the mutation of Ser-505 to Ala is known to block cPLA$_2$ activation by members of the MAP kinase family (Lin et al., 1993), the functional relevance of Ser-727 has not been reported.

Several lines of evidence suggested that cPLA$_2$ may be a member of the $\alpha/\beta$ hydrolase family. These enzymes possess a common core that consists of a well-conserved mixed $\beta$ sheet whose strands are interspersed by $\alpha$ helices and employ a catalytic triad similar to the one present in serine proteases (Schrag and Cygler, 1997). The catalytic mechanism of cPLA$_2$ proceeds through a serine-acyl intermediate (Reynolds et al., 1993; Trimble et al., 1993; Hanel and Gelb, 1995) using Ser-228 as the nucleophilic residue (Sharp et al., 1994; Huang et al., 1996). This serine is present in a pentapeptide sequence, G-L-S-G-S, which is similar to the classic "lipase motif" G-X-S-X-G (Schrag and Cygler, 1997) found in $\alpha/\beta$ hydrolases. The catalytic serine of these enzymes is present in a tight turn between a $\beta$ strand and an $\alpha$ helix, termed the "nucleophilic elbow" (see review by Schrag and Cygler, 1997). This arrangement forces the serine residue to adopt unusual main chain $\phi,\psi$ torsion angles and requires that the $+2$ and $-2$ side chains be small to avoid steric clash, thus the prevalence of the G-X-S-X-G motif (Derewenda and Derewenda, 1991).

In addition to Ser-228, Asp-549 was shown to be essential for cPLA$_2$ activity. However, none of the 19 histidine residues were enzymatically relevant (Pickard et al., 1996). A different residue, Arg-200, was shown to be required for catalysis, suggesting that cPLA$_2$ may employ a novel mechanism.

*To whom correspondence should be addressed (e-mail: adessen@genetics.com [A. D], wsomers@genetics.com [W. S. S.]).

Table 1. Statistics for Data Collection, Phase Determination, and Refinement

| Data Collection | | | | | | | | | |
|---|---|---|---|---|---|---|---|---|---|
| | Native | | Peak | | Inflection | | Descending Edge | | |
| Wavelength (Å) | $\lambda = 1.20$ | | $\lambda_1 = 1.64902$ | | $\lambda_2 = 1.64963$ | | $\lambda_3 = 1.64834$ | | |
| Max. resolution (Å) | 2.5 | | 3.4 | | 3.3 | | 3.2 | | |
| $R_{sym}$ (%)[a] | 6.4 (30.0) | | 11.2 (41.5) | | 10.3 (37.1) | | 9.0 (38.6) | | |
| % completeness | 93.3 (87.9) | | 99.6 (99.4) | | 99.7 (99.5) | | 99.6 (99.5) | | |
| Total reflections | 271,686 | | 195,666 | | 213,851 | | 233,142 | | |
| Unique reflections | 66,223 | | 54,331[b] | | 59,265[b] | | 64,885[b] | | |
| $<I/\sigma(I)>$ | 18.2 (3.3) | | 9.9 (2.6) | | 12.3 (3.3) | | 13.3 (2.8) | | |
| f′ (e−)[c] | | | −9.89 | | −17.50 | | −1.86 | | |
| f″ (e−) | | | 31.90 | | 18.63 | | 19.24 | | |
| **MAD Phasing** | | | | | | | | | |
| Resolution limits (Å) | 9.67 | 6.70 | 5.44 | 4.69 | 4.18 | 3.81 | 3.53 | 3.37 | Overall |
| Phasing power[d] | | | | | | | | | |
| $\lambda_2$ | 3.26 | 4.08 | 3.65 | 2.84 | 2.07 | 1.48 | 1.11 | 0.93 | 2.24 |
| $\lambda_1$ isomorphous | 1.20 | 1.15 | 1.05 | 0.83 | 0.75 | 0.68 | 0.63 | 0.53 | 0.83 |
| $\lambda_1$ anomalous | 3.25 | 4.26 | 3.89 | 3.18 | 2.37 | 1.70 | 1.30 | 1.21 | 2.59 |
| $\lambda_3$ isomorphous | 0.98 | 1.20 | 1.24 | 1.32 | 1.39 | 1.39 | 1.35 | 1.28 | 1.30 |
| $\lambda_3$ anomalous | 3.18 | 4.01 | 3.58 | 2.99 | 2.30 | 1.66 | 1.26 | 1.07 | 2.34 |
| Mean FOM[e] | 0.77 | 0.75 | 0.70 | 0.63 | 0.55 | 0.44 | 0.35 | 0.29 | 0.51 |
| **Model Refinement** | | | | | | | | | |
| Resolution (Å) | 12.0–2.5 | | | | | | | | |
| R factor (%)[f] | 22.9 | | $R_{free}$ (%) | | 29.8 | | <B value> (Å$^2$) | | 47.7 |
| Rms deviations from ideal geometry | | | | | | | | | |
| Bonds (Å) | 0.016 | | | | | | | | |
| Angles (°) | 1.94 | | | | | | | | |
| B values (Å$^2$) | 6.7 | | | | | | | | |

[a] $R_{sym} = \Sigma\ |I_h - <I_h>|/\Sigma I_h$, where $<I_h>$ is the average intensity over symmetry equivalents. Numbers in parentheses reflect statistics for the last shell.

[b] Friedel pairs separate.

[c] f′ and f′′ reported values were refined by SHARP.

[d] Phasing power $= \Sigma|F_H|/\Sigma||F_{PHobs}| - |F_{PHcalc}||$, where $F_H$ is the calculated heavy atom structure factor amplitude.

[e] Figure of merit $= <|\Sigma P(\alpha)e^{i\alpha}/\Sigma|P(\alpha)|>$, where $\alpha$ is the phase and $P(\alpha)$ is the phase probability distribution.

[f] $R = \Sigma||F_{obs}| - |F_{calc}|/\Sigma|F_{obs}|$, where $R_{free}$ is calculated for a randomly chosen 10% of reflections and R factor is calculated for the remaining 90% of reflections ($F > 2.0$) used for structure refinement.

Like both the 14 kDa secreted $PLA_2$s and the lipases of the $\alpha/\beta$ hydrolase family, $cPLA_2$ preferentially cleaves substrates presented at a membrane interface rather than in monomeric form (Nalefski et al., 1994). This phenomenon, known as interfacial activation, has been attributed to both localized conformational changes in the lipases of the $\alpha/\beta$ hydrolase family and, in the case of secreted $PLA_2$s, more favorable presentation of the substrate (Scott et al., 1990). To date, no experiments have provided insight into $cPLA_2$'s 1500-fold preference for substrate at an interface.

Despite the key role of $cPLA_2$ in inflammatory disease, its three-dimensional structure remained unsolved, leaving numerous questions unanswered. Here, we report the X-ray crystal structure of human $cPLA_2$ at 2.5 Å resolution. The structure provides insight into the origin of arachidonate selectivity and interfacial activation, clarifies the roles of Ser-228, Asp-549, and Arg-200, and reveals the interplay between the C2 and catalytic domains. Unexpectedly, the structure is of a unique topology, distinct from that of the $\alpha/\beta$ hydrolase family.

## Results

### The Structure of $cPLA_2$ Was Solved by Employing One Heavy Atom Scatterer Per 749 Residues

Full-length human $cPLA_2$ was expressed in CHO cells as described in Experimental Procedures. Crystals were obtained at 18°C using PEG 1000 as a precipitant and employing standard vapor diffusion techniques. Single crystals grew within a few days to dimensions of up to 0.6 mm × 0.5 mm × 0.1 mm and diffracted to a minimum Bragg spacing of 2.5 Å. Crystals are of space group $P2_12_12$ (a = 153.59 Å, b = 95.49 Å, c = 139.13 Å), with two monomers (1498 residues) and 60% solvent per asymmetric unit.

Attempts to prepare heavy atom–soaked crystals of $cPLA_2$ revealed that only gadolinium or terbium could generate isomorphous derivatives. Either lanthanide replaced a single $Ca^{2+}$ atom in the C2 domain, thus providing a single heavy atom scatterer per 749 amino acid residues. In-house phasing information from these crystals was not of high enough quality to produce an interpretable electron density map. This observation, added to the fact that binding of most heavy atoms generated nonisomorphism between native and soaked crystals, led to an effort to solve the structure of $cPLA_2$ by multiwavelength anomalous dispersion (MAD) phasing (Hendrickson, 1991).

Data at three different wavelengths around the Tb $L_{III}$ edge (see Table 1) were collected from a single Tb-treated crystal. Experimental phases to 3.2 Å were subsequently modified by solvent flattening and noncrystallographic symmetry averaging and extended to 2.5 Å. This procedure generated an electron density map of extraordinary quality (Figure 1) in which both domains

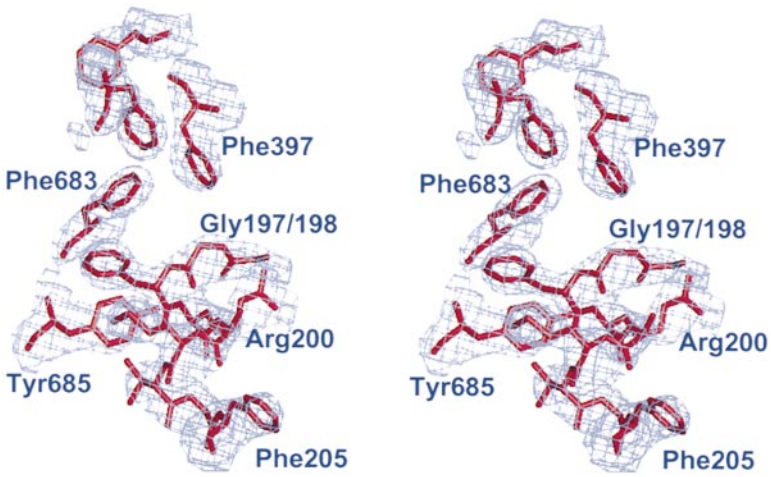


Figure 1. Experimental Map Generated with MAD Phases Obtained from Scattering of a Single Tb Atom Per 749 Residues of cPLA$_2$

Solvent flattening (60% solvent content) and two-fold noncrystallographic symmetry averaging were employed for map generation.

of each cPLA$_2$ monomer could be clearly identified. The present model contains 1260 residues (between both monomers) and 48 water molecules.

**Molecular Structure**

The cPLA$_2$ monomer is a two-domain ellipsoidal structure with dimensions of ~100 Å × 55 Å × 45 Å (Figure 2A). The N-terminal domain (residues 16–138) is a β sandwich of the C2 family (Nalefski and Falke, 1996), connected by residues 139–143 to the catalytic domain, with which it forms very few protein–protein contacts. The central core of the catalytic domain is composed of a 10-strand central β sheet with interspersed helices, and its topology is unexpectedly distinct from that of the canonical α/β hydrolase fold. The cPLA$_2$ monomers present in the asymmetric unit are not perfectly superimposable due to flexibility of the interdomain loop; superposition of the C2 domains leads to a 4°–5° difference between the two catalytic domains. The interdomain loop has a slightly different conformation in each monomer, and its residues display high temperature factors.

cPLA$_2$ is a cytosolic protein that binds to its target membrane through its C2 domain when intracellular levels of $Ca^{2+}$ are raised (Clark et al., 1991). The domain arrangement of cPLA$_2$ suggests how the active site is oriented with respect to the cellular membrane. Figure 2B is a surface diagram that highlights results of HSQC studies performed on the C2 domain by Xu and coworkers (1998). Residues that displayed $N^{15}$/NH shifts upon binding to dodecylphosphocholine micelles in these experiments are highlighted in purple. It is clear that the highlighted residues appear on the same face of the molecule as the active site. Consequently, if the C2 domain employs these residues to associate with a phospholipid membrane, the catalytic domain is roughly positioned to bind a phospholipid substrate in the active site. The flexibility of the linker between the two domains as well as the lack of major protein–protein interactions between them suggests that a small rotation between domains can occur to optimize interactions with the membrane.

As shown in the surface potential diagram in Figure 2C, a highly basic region extends from the active site through a strip of positively charged residues on the β3 strand of the C2 domain (Arg-57 and Arg-59). Residues 434–456, however, are disordered (see Figure 5A), making it impossible to accurately define the true size of the basic patch. Nevertheless, it is noteworthy that similar basic patches were seen in PI4 kinase and in different species of secreted PLA$_2$s (Rao et al., 1998). It is tempting to suspect that the high-affinity binding of cPLA$_2$ to membranes made of phosphatidyl methanol (Hixon et al., 1998) is mediated through this region.

**The N-Terminal C2 Domain**

The structure of the C2 domain in full-length cPLA$_2$ is very similar to those solved by NMR and X-ray crystallography (Xu et al., 1998; Perisic et al., 1998), with minor differences. Briefly, it consists of eight antiparallel β strands interconnected by six loops, folding into a β sandwich that fits the "type II" topology for C2 domains (Nalefski et al., 1994). Two $Ca^{2+}$ atoms, spaced 4 Å apart, are bound at one end of the C2 domain through a constellation of Asp and Asn side chains and backbone carbonyl atoms on three distinct loops; the same atomic arrangement has been observed in the C2 domain solved by Perisic and coworkers (1998). The environment of the $Ca^{2+}$ atoms in full-length cPLA$_2$, however, does not display the same water molecules present in the C2 structure solved by these authors. Instead, coordinated to calcium site 1 (defined in Perisic et al., 1998) is a molecule of MES (2-[N-morpholino] ethanesulfonic acid) from the buffer employed in crystallization and cryoprotection. In both cPLA$_2$ monomers, the distance between $Ca^{2+}$ 1 and the closest MES sulfonate oxygen atom is approximately 2.2 Å. In addition, the morpholino group is also in contact with the side chains of His-62 and Tyr-96, which form a small hydrophobic niche. Although a crystallization artifact, the coordination of $Ca^{2+}$ 1 of cPLA$_2$ to the sulfate group of MES could be emulating the binding mode of the phosphate group of a phospholipid molecule.

**The Novel Topology of the cPLA$_2$ Fold Distinguishes It from α/β Hydrolases**

The catalytic domain of cPLA$_2$ is composed of 14 β strands and 13 α helices; its central core consists of a 10-stranded central mixed β sheet surrounded by 9 α helices with strands β4, β5, β10, β11, and β12 forming the most obvious portion of the sheet (see Figure 2A

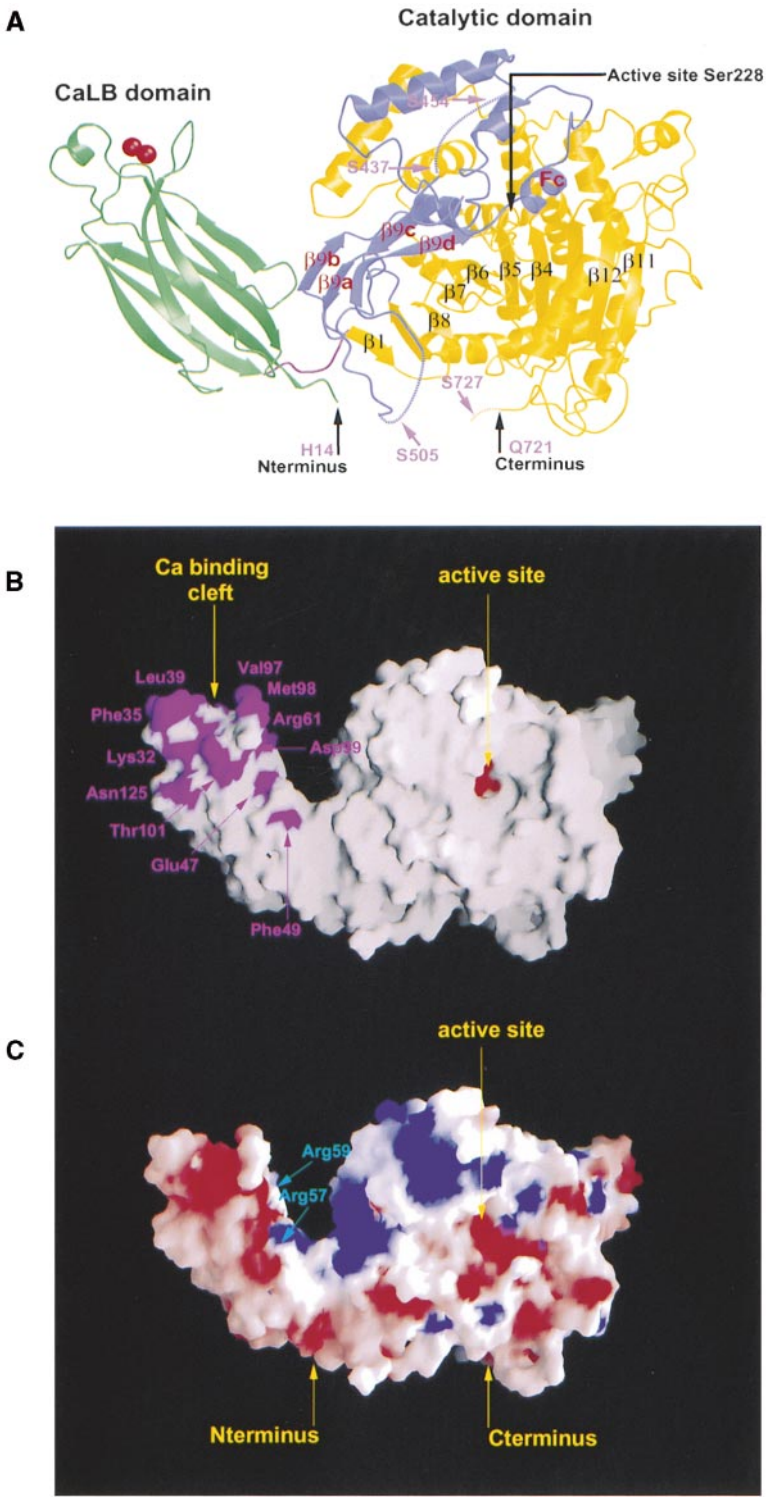


Figure 2. Ribbon and Surface Diagrams of $cPLA_2$

(A) Ribbon diagram of the $cPLA_2$ monomer. The C2 domain is shown in green, with the two $Ca^{2+}$ atoms depicted in red. The "cap" structure of $cPLA_2$ is colored purple. Mobile loops with poor electron density are shown as dots. The flexible linker between the C2 and catalytic domains is colored red. The positions of the four serine residues, which are phosphorylated in $cPLA_2$, are also shown. For clarity, β9 and β10 have not been labeled; β10 lies between β4 and β12. Figure prepared with MOLSCRIPT (Kraulis, 1991) and RASTER3D (Bacon and Anderson, 1988).

(B) GRASP surface diagram of $cPLA_2$. Residues that presented N15/NH shifts upon interaction with dodecylphosphocholine micelles in NMR experiments by Xu et al. (1998) are colored purple. The $cPLA_2$ active cleft is highlighted in red. Lid residues (413–457) have been removed for clarity.

(C) Surface potential representation of $cPLA_2$, with regions with electrostatic potential $<-3.5$ $k_BT$ are red, while those $>+3.5$ $k_BT$ are blue ($K_B$, Boltzmann constant; T, absolute temperature). The lid residues (413–457) have been removed for clarity, and neither calcium nor MES was employed in the generation of the potential. A highly basic patch is clearly visible on the membrane-binding region of the molecule and also encompasses residues 57–61, which are located on the β3 strand of the C2 domain. Figure prepared with GRASP (Nicholls, 1992). All views are in the same orientation, with the plasma membrane coming from the direction of the eyes of the reader.

and the Richardson diagram in Figure 3B). The β sheet has a superhelical twist with β6 and β11 lying approximately 90° to one another. For simplicity, the secondary elements of $cPLA_2$ have been identified based on the α/β hydrolase fold nomenclature presented by Schrag and Cylger (1997), in which the catalytic serine is preceded by β5 and followed by helix C.

The first β strand in the $cPLA_2$ core is β1, which follows the flexible connection after the C2 domain. A loop containing one long helix makes the connection to β4, in the central part of the fold. The following parallel β strand, β5, precedes the catalytic serine (228). The topology of β5, helix C (colored pink in Figures 3A and 3B), and of their interconnecting loop is similar to that

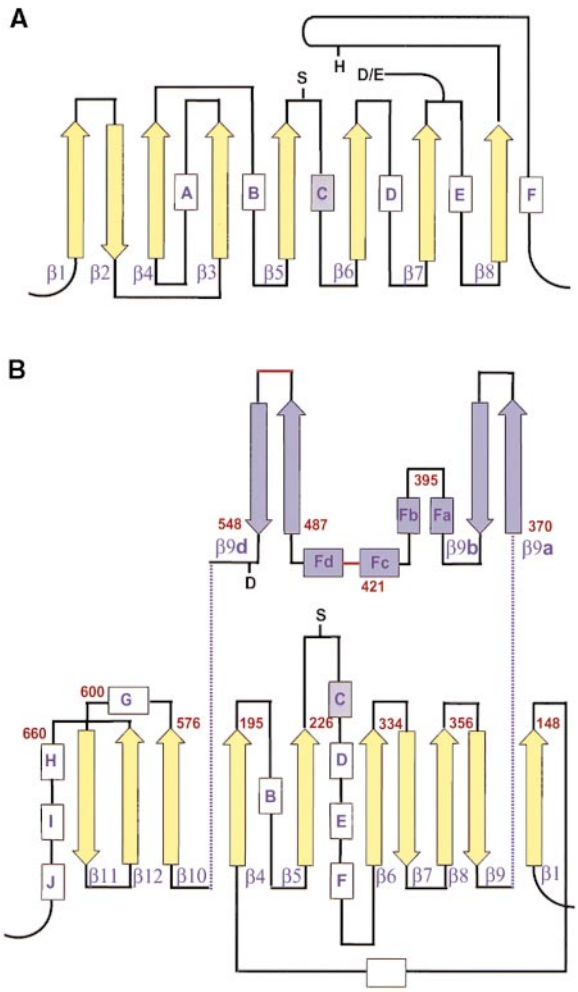


Figure 3. Richardson Diagrams of cPLA$_2$ and the Canonical α/β Hydrolase Fold

(A) Richardson representation of the canonical α/β hydrolase fold. β strands are represented as arrows, while α helices are rectangles. Secondary structural element numbering is according to the review by Schrag and Cygler (1997). Helix C, which immediately follows the "nucleophilic elbow," is colored pink.

(B) Richardson diagram of the cPLA$_2$ fold. The naming scheme was devised so that the helix immediately following Ser-288 is helix C, as in the canonical α/β hydrolase fold. The central core is colored yellow for a more facile comparison with the canonical α/β hydrolase fold in (A). Elements composing the "cap" are colored purple; loop regions in red are highly mobile and do not present traceable electron density. Lid residues (see text) are represented primarily by helix Fc.

seen in α/β hydrolases. This interconnecting loop is termed the "nucleophilic elbow." Three more α helices, interwoven by loops, provide the connection between this region and the further four β strands of this part of the fold (β6–β9).

After β9 there is a major divergence from the central α/β core. The cPLA$_2$ sequence at this point forms the region shown in purple in Figures 2A and 3B. This 180-residue patch forms a catalytic domain "cap." Asp-549, the catalytic partner of Ser-228, immediately follows β9d. Following the cap structure, the last three β strands (β10, β11, and β12) are positioned as to complete the central β sheet and are interspersed by helices G to J.

The α/β hydrolase fold is common to many esterases and other hydrolytic enzymes (Derewenda and Derewenda, 1991; Schrag and Cygler, 1997). Its Richardson diagram (Figure 3A) consists of a central β sheet whose order of β strands follows the sequence linearly (with the exception of β3, which is often placed between β4 and β5). At first glance, the topology of cPLA$_2$ appears to be a circular permutation of the α/β hydrolase fold. However, a careful comparison of Figures 3A and 3B clearly reveals that only the region encompassing the nucleophilic elbow is in fact directly comparable (β5 to helix C; residues 222–238). Major distinctions include the antiparallel nature of strands β6 to β9, the multiplicity of helices between β5 and β6, and the absence of intervening helices between strands of the latter part of the cPLA$_2$ α/β core.

Although the cap structure in cPLA$_2$ (residues 370–548) is part of the catalytic domain, it is not included in the α/β core. cPLA$_2$ displays 30% identity in its catalytic domain with two other lipases, cPLA$_2$s β and γ (Underwood et al., 1998; C. Song et al., unpublished data), and their sequence comparisons (Figure 4) show that homology is concentrated within the α/β core (yellow elements) and β strand 9a and α helix Fa. Thus, the central part of the cap is distinct among cPLA$_2$ isoforms. A comparison between the ribbon diagram of cPLA$_2$ in Figure 2A, in which the cap region is displayed in purple, and the surface potential diagram in Figure 2C reveals that the highly basic region hypothesized above as making electrostatic contacts with membrane phospholipids is in fact formed in large part by cap residues.

The cap region of cPLA$_2$ also contains two of the three most mobile regions of the entire structure, residues 433–456 and 500–536; the third region is the C terminus, residues 722–749. These amino acid stretches do not have traceable electron density and are not included in the model (dotted lines in Figure 2A). Interestingly, it is these highly flexible regions of the cap that harbor three of the four serine residues that become phosphorylated upon agonist stimulation (437, 454, and 505). The role of Ser-437 and Ser-454 is unclear, since they are not conserved among different species. In contrast, Ser-505 is conserved in cPLA$_2$ from evolutionarily distinct species (chicken, human, zebrafish, mouse, and rat), and its phosphorylation by MAP kinase is required for maximal activation of cPLA$_2$ (Lin, et al., 1993; Qiu et al., 1998). Ser-505, which in our crystals may be heterogeneously phosphorylated and is located in a highly flexible, solvent-exposed loop, makes no contacts either with the body of the protein or other neighboring cPLA$_2$ monomers in the lattice. The fourth site of cPLA$_2$ phosphorylation, Ser-727, is at the C terminus of the structure. Although this site is conserved among species, its functional relevance is not yet known (Qiu et al., 1998).

A recent report describing dramatic activation of cPLA$_2$ by phosphatidylinositol 4,5-bisphosphate led to the suggestion that cPLA$_2$ may contain a pleckstrin homology domain (Mosior et al., 1998). Analysis of our structure reveals no region with similarity to a pleckstrin homology domain.

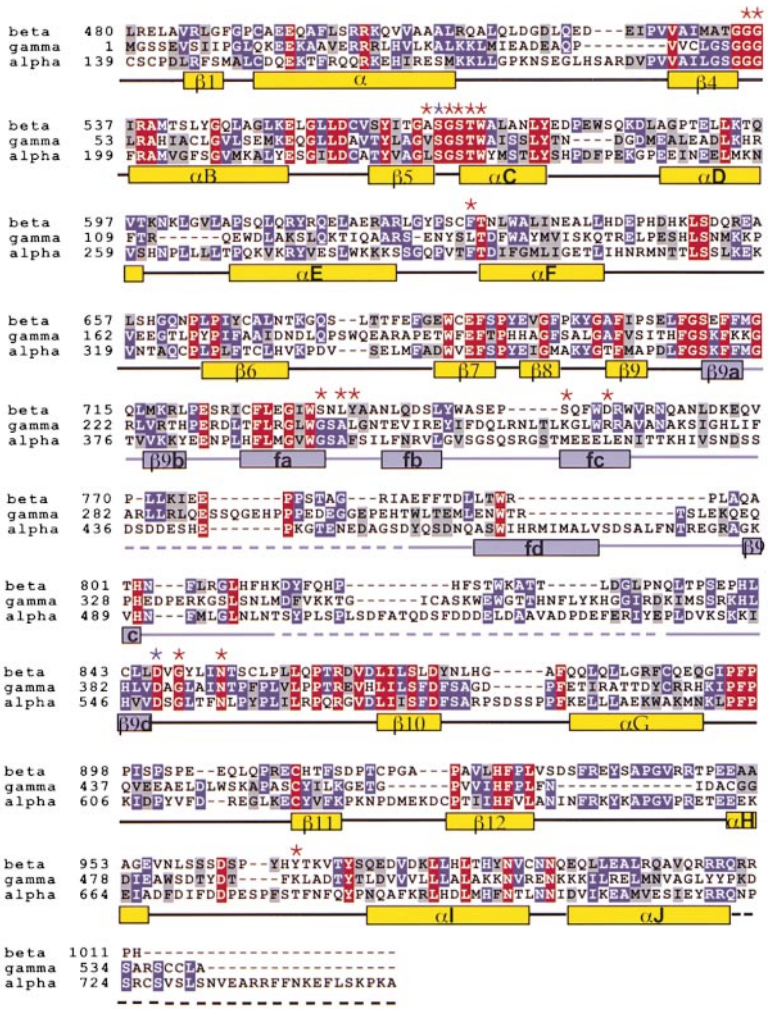


Figure 4. Primary Structure Alignment of cPLA$_2$ α, β, and γ

Secondary structural elements observed in the X-ray crystal structure of cPLA$_2$ α are indicated below the sequences and are color coded as components of the cap region (purple) or main fold (yellow). Lines represent areas of turns or loops. Residues identified with dotted lines do not display traceable electron density. The asterisk identifies residues lining the active site or present in the lid.

### A Deep Active Site Funnel Is Partially Covered by a Solvent-Accessible Lid

The most remarkable feature of the cPLA$_2$ structure is the active site funnel, which penetrates one-third of the way into the catalytic domain to reveal Ser-228 and Asp-549 placed at the bottom of a deep, narrow cleft. Although wide at the top, the funnel narrows to an approximate diameter of 7 Å at the mouth of the active site cleft visible in Figure 5A. The funnel is lined with hydrophobic residues (blue in Figure 5A) and forms a cradle into which fatty acyl moieties of membrane phospholipid substrates may bind. The 8 Å distance between the O$\gamma$ of Ser-228 and the top of the active site cleft is enough to accommodate up to the first *cis* double bond of a bound arachidonyl substrate, even in the most extended conformation of the molecule.

Attempts to model a diacylphospholipid molecule in the active site cleft of cPLA$_2$ demonstrated that the acyl ester bond cannot be positioned in the vicinity of Ser-228 without the fatty acid chains clashing with residues located directly above it (Figure 5A). These residues, which partially block access to the active site, appear to be part of a "lid" composed of amino acids 413–457. The lid folds into a loop region, followed by a small helix (Fc; Figure 3B) and a short turn. Residues 408–412, which lead into the lid region, display large temperature factors, and residues 434–456 do not possess traceable electron density. These observations suggest that both of these regions are highly mobile and could be envisioned as "lid hinges." Given this flexibility, it is likely that the lid is in a different conformation when substrate is bound. Notably, the visible region of the lid is amphipathic; its solvent-exposed face is formed primarily by polar residues (T416, E418, E419, E420, and N423), while the inner side is lined with hydrophobic amino acids (M417, L421, and I424).

X-ray crystallography has yielded multiple examples of lipases that exist in both "closed lid" and "open lid" forms, the latter crystallized in the presence of substrate or inhibitors (Cygler and Schrag, 1997). Lipases that exist in both forms are known to undergo a phenomenon termed interfacial activation, in which catalytic activity is greater in the presence of micellar rather than monomeric substrates. Likewise, cPLA$_2$ undergoes such activation. It is possible that movement of the cPLA$_2$ lid exposes both the active site and a greater hydrophobic surface, which could be stabilized by interacting with the membrane.

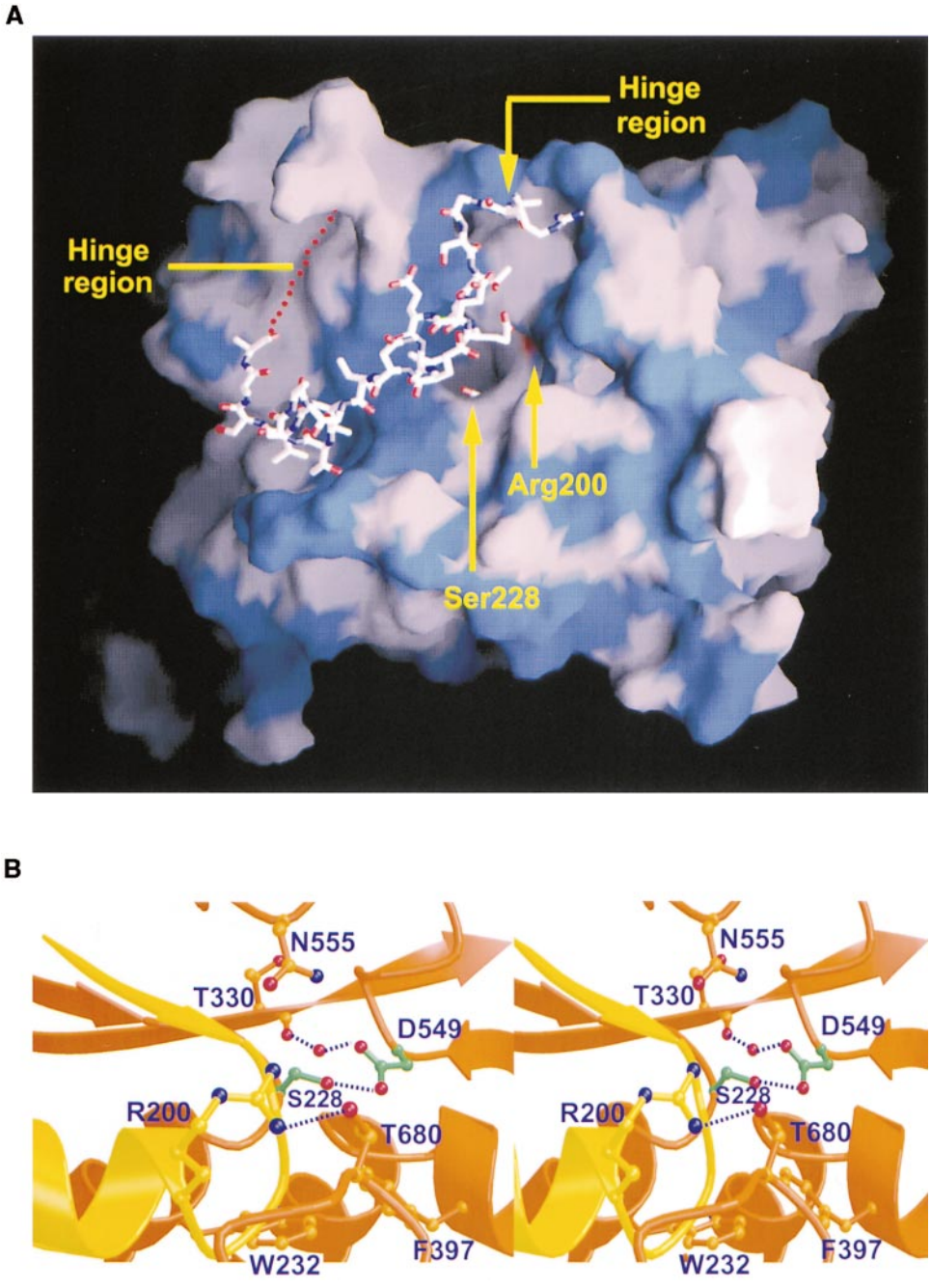


Figure 5. Catalytic Domain and Active Site of cPLA$_2$

(A) Surface diagram showing the catalytic domain of cPLA$_2$ covered by the lid residues. Ser-228 is shown at the bottom of the funnel. The continuation of the sequence not visible in experimental maps is represented by red dots and is proposed to be involved in the formation of a lid hinge. Residues for which only the backbone atoms are visible in electron density maps are represented as alanines. Exposed surfaces of all hydrophobic residues have been colored blue, and that of Arg-200 has been colored red. The figure was prepared with GRASP (Nicholls, 1992).

(B) Close-up of the active site of cPLA$_2$. The two residues involved directly in catalysis are colored green. Arg-200 and the loop harboring Gly residues 197 and 198 are shown in yellow. A single water molecule visible in the experimental maps hydrogen bonds with Asp-549 and a carbonyl oxygen from Thr-330. Figure generated with MOLSCRIPT and RASTER3D.

**Catalysis by cPLA$_2$ Proceeds via a Mechanism Distinct from that of Other Acyl Hydrolases**

Acyl hydrolysis by $\alpha/\beta$ hydrolases is performed by a catalytic triad (Ser-His-Asp/Glu) analogous to the one present in serine proteases, where the histidine residue is spatially positioned between the serine and the aspartate. Histidine, activated by aspartate, abstracts the serine proton during its nucleophilic attack on the substrate

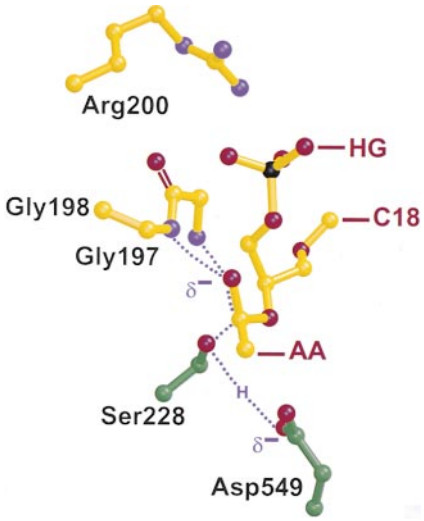


Figure 6. Transition-State Complex Proposed for cPLA$_2$, Involving the Attack of Ser-228 on the *sn*-2 Position of the Substrate

Phosphate atoms are shown in black; residues involved in catalysis are depicted in green. Gly-197 and 198 are suggested as being part of the oxyanion hole, while Arg-200 stabilizes the phosphate moiety of the head group. AA, arachidonic acid; HG, head group; C18, octadecyl group.

ester bond. Although a similar mechanism was anticipated for cPLA$_2$, site-directed mutagenesis (Sharp et al., 1994; Pickard et al., 1996) identified Ser-228 and Asp-549 as essential for catalysis, but none of the 19 histidine residues were required for activity. Surprisingly, mutagenesis of Arg-200 to either lysine or alanine had a dramatic effect. These observations suggested several novel catalytic mechanisms, including one in which Arg-200 replaced histidine in the catalytic triad (Pickard et al., 1996).

However, instead of the expected triad, the X-ray crystal structure of cPLA$_2$ clearly reveals an active site dyad in which the O$\gamma$ atom of Ser-228 is only 2.9 Å from O$\delta$2 of Asp-549. The guanidinium group of Arg-200 is 9 Å away from Ser-228 O$\gamma$, and all histidines are outside of a 10 Å radius. All polar interactions within a 3.5 Å range of either Asp-549 or Ser-228 are made by backbone groups or a lone water molecule positioned 3.2 Å away from Asp-549 O$\delta$1 (Figure 5B). Although Asn-555 lines the active site funnel, its N$\delta$2 atom is approximately 6 Å away from either residue.

In proteases and lipases, certain amide backbone atoms within the cleft are often positioned to stabilize the negative charge that develops upon nucleophilic attack by serine and are thus termed the "oxyanion hole." Analysis of the electron density map in the region of Ser-228 showed that the peptide bonds of residues Gly-197 and Gly-198 are in an approximate *cis* configuration. In this orientation, both amide protons are appropriately positioned to stabilize a developing oxyanion. In addition, the backbone amide group of Gly-229, located in the nucleophilic elbow, may also be part of the oxyanion hole. Consequently, this region appears to be well designed to stabilize the transition state generated by nucleophilic attack by Ser-228.

Although it is clear from the crystal structure that the guanidinium group of Arg-200 is not part of the catalytic triad, its role remains uncertain. Its location near the mouth of the active site cleft appropriately positions it to interact with the phosphate moiety of the substrate. However, Pickard et al. (1996) reported that the activity of cPLA$_2$ toward a non–phosphate-containing substrate (arachidonic acid ester of 7-hydroxycoumarin) was also greatly reduced by mutagenesis of Arg-200, thus suggesting that this residue may serve multiple purposes.

It is noteworthy that Arg-200 is located on the same loop as Gly-197/198 of the oxyanion hole and its side chain hydrogen bonds with Thr-680 and with the backbone carbonyl oxygen atoms of Phe-576 and Phe-678. The lack of these hydrogen bonds in the Arg-200 Lys mutant reported by Pickard and coworkers (1996) could be responsible for subtle alterations in the conformation of the oxyanion hole loop with dramatic consequences on activity.

Based on our crystal structure and other biochemical experiments showing evidence of a serine-acyl intermediate in cPLA$_2$ catalysis, we propose a mechanism for cPLA$_2$ (see Figure 6). After calcium-dependent membrane translocation, an individual substrate molecule can diffuse into and bind in the narrow cleft of the active site such that its *sn*-2 ester bond is close to Ser-228. The phosphate moiety of the head group is stabilized by the Arg-200 side chain, and both fatty acyl chains can be directed back toward the top of the cleft. Following formation of the enzyme–substrate complex, Asp-549 activates Ser-228 by abstracting a proton during its nucleophilic attack at the *sn*-2 ester. An oxyanion hole formed by the backbone amide groups of Gly-197 and Gly-198 polarizes the *sn*-2 ester and stabilizes the transition state of the developing tetrahedral intermediate. The serine-acyl intermediate is generated upon collapse of the tetrahedral intermediate with transfer of a proton from Asp-549 to the leaving lysophospholipid. Hydrolysis of the acyl intermediate by water then occurs through an analogous mechanism. cPLA$_2$ may then either dissociate from the membrane interface or bind another phospholipid substrate, repeating the cycle.

Although a nucleophilic serine in the absence of a catalytic triad is unusual, it is observed in both class A TEM-1 $\beta$-lactamase (Matagne et al., 1998) and penicillin acylase (Duggleby et al., 1995). In the case of $\beta$-lactamase, Ser-70 is activated by Glu-166 with the participation of a bridging water molecule. In the catalytic mechanism of penicillin acylase, the N-terminal serine is activated by its own $\alpha$-amino group, again through a bridging water. Thus, cPLA$_2$ is a third distinct example of an acylase using a nucleophilic serine without a complete catalytic triad.

## Discussion

Since leukotrienes, prostaglandins, and PAF play significant roles in the pathophysiology of major diseases (Bonventre et al, 1997; Uozumi et al., 1997), it is important to understand the three-dimensional structure of cPLA$_2$, an enzyme central in their biosynthesis. The cPLA$_2$ fold clearly shows that the enzyme consists of two distinct, independently folded domains. This result was not unexpected based on earlier work in which the

C2 and catalytic domains were fully functional when expressed independently (Nalefski et al., 1994, 1998). However, the sparsity of contacts between the domains was surprising. The only residue in the catalytic domain of cPLA$_2$ observed to directly contact C2 is Lys-371, which forms a salt bridge with Asp-55. In addition, the high temperature factors and distinct conformation of the interdomain linker in the two monomers in the cPLA$_2$ asymmetric unit are a further indication of flexibility between the domains.

Although C2 domains are commonly observed in signaling molecules, the C2 domains of PLC$\delta$1 and now cPLA$_2$ are the first to be reported in the context of a catalytic domain (Essen et al., 1996; Grobler et al., 1996). In contrast to cPLA$_2$, extensive hydrophobic contacts exist between the PLC$\delta$1 domains, indicating a fixed orientation. In both PLC$\delta$1 and cPLA$_2$, the calcium binding loops of the C2 domains are thought to interact with the membrane surface (Grobler et al., 1996; Nalefski and Falke, 1998; Perisic et al., 1998; Xu et al., 1998). Superposition of the C2 domains of both PLC$\delta$1 and cPLA$_2$ reveal that their catalytic sites are both facing the membrane surface. However, they are rotated by approximately 10°–20° with respect to one another, suggesting that a slight reorientation of the cPLA$_2$ domains may be critical for appropriate membrane positioning. It is noteworthy that Ser-505, which is essential for optimal activity in cells, is located near the interdomain linker region. Although far from certain, it is possible that phosphorylation of Ser-505 favors an optimal orientation between the C2 and catalytic domains of cPLA$_2$.

The detailed comparison of the structure of cPLA$_2$ and the classic $\alpha/\beta$ hydrolase fold clearly argues that cPLA$_2$ contains a novel topology. However, as noted earlier, the $\beta$ hairpin containing the active site serine is structurally analogous to the "nucleophilic elbow" of the $\alpha/\beta$ hydrolase fold. It should be noted that serines present in G-X-S-X-G motifs in proteases do not share this same conformation (Derewenda and Derewenda, 1991). A Blast search (Altschul et al., 1997) of the cPLA$_2$ catalytic domain shows a short region of homology with phospholipase B's and lysophospholipases that include Gly-197/198 of the oxyanion hole Arg-200 and the cPLA$_2$ lipase motif, which contains Ser-228. The high homology in the short region is also consistent with the genomic structure, since these residues are encoded by a single exon (Bonventre et al., 1997; Uozumi et al., 1997).

Two mechanisms could be proposed for cPLA$_2$ employing Ser-228 and Asp-549 for catalysis. In one mechanism, Asp-549 could act as an acid catalyst, hydrogen bonding to the carbonyl of the *sn*-2 ester without directly interacting with Ser-228. However, the crystal structure clearly shows that Asp-549 is ideally positioned to act as a general base, directly activating Ser-228. Thus, we propose the transition state shown in Figure 6. Although it is difficult to compare the efficiency of this catalytic dyad to the traditional Ser-His-Asp triad of the $\alpha/\beta$ hydrolases and serine proteases, it is the activation energy required to reach the transition state that is important in catalysis. Thus, any energetic deficiencies inherent to the dyad may be offset by very strong hydrogen bonds between the developing negative charge on the carbonyl oxygen and the oxyanion hole (Cleland and Kreevoy, 1994).

The selectivity for arachidonyl-containing phospholipids is a distinguishing feature of cPLA$_2$ (Hanel and Gelb, 1993; Clark et al., 1995). This selectivity can originate either in a substrate-driven or an enzyme-driven scenario. In the first scenario, the polyunsaturation of the arachidonyl phospholipids ensures looser packing and thus greater exposure of the scissile *sn*-2 ester bond located at the membrane–water interface. In this case, one would expect the catalytic machinery of cPLA$_2$ to be on the surface of the enzyme, where it could act without extracting the lipid from the bilayer. This situation would be analogous to the one presented by the flattened kinase domain of Type IIb phosphatidylinositol phosphate kinase, where the enzyme phosphorylates phosphatidylinositol in situ (Rao et al., 1998). In contrast, in the enzyme-driven scenario, the phospholipid is extracted from the membrane such that the *cis* double bonds of the *sn*-2 fatty acid are in direct contact with the active site. The structure reported in this work clearly demonstrates that arachidonic acid selectivity is enzyme driven, since the active site serine lies in a cleft so deep that at least the 5-*cis* double bond remains in the cleft even in the fatty acid's most extended conformation. This particular double bond has been shown to be the most relevant for cPLA$_2$ arachidonate selectivity (Hanel and Gelb, 1995).

The level of identity between cPLA$_2$ $\alpha$ and $\gamma$ allows us to confidently identify the residues in cPLA$_2$ $\gamma$ that line the active site. This analysis shows that only two residues differ within the cleft. Although these changes may be responsible for the much lower arachidonyl selectivity shown by cPLA$_2$ $\gamma$ (Underwood et al., 1998), there is no homology between lid residues of cPLA$_2$ $\alpha$ and $\gamma$. It will be informative to mutate the residues that are distinct between $\alpha$ and $\gamma$ cPLA$_2$s in order to determine residues responsible for selectivity.

The conformation of cPLA$_2$ shown in this structure must represent the "closed" form of the enzyme, since the fatty acyl chains of a substrate modeled into the active site cleft clash with the lid residues. We expect that, upon membrane binding, the lid must move to allow active site access, consistent with the interfacial activation noted for cPLA$_2$ upon binding to the membrane interface (Nalefski et al., 1994). This phenomenon of lid movement and interfacial activation has been noted for numerous lipases (Cygler and Schrag, 1997). Lid movement in many of these enzymes increases the exposed hydrophobic surface. The amphipathic nature of the lid in cPLA$_2$ suggests that the enzyme can change from a soluble, closed conformation to an open, more hydrophobic form stabilized by membrane binding.

Although we cannot comment on the conformation of the lid or hinge regions in the open form, it is clear from Figure 5A that the semicircular rim of the active site funnel is raised (approximately 7 Å) above the mouth of the active site cleft. If this rim were to rest on the membrane surface, it would require the substrate to traverse solvent-filled space before reaching the cleft. Consequently, we propose that the rim residues are at least partially imbedded in the membrane interface, consistent with the prevalence of hydrophobic residues at this location. The charged residues that lie between the active site cleft and the rim may interact with phospholipid head groups. The extent of penetration proposed also

places the basic patch obvious in Figure 2C proximal to the membrane surface. This membrane-binding model is consistent with the increased affinity of $cPLA_2$ for anionic lipids (Hixon et al., 1998) as well as its inhibition by sphingomyelin, whose rigid structure would disfavor interface penetration (Leslie and Channon, 1990).

## Experimental Procedures

### Protein Production, Crystallization, and Data Collection

Full-length human $cPLA_2$ (residues 1–749) was expressed in E5-CHO cells as described in Lin et al. (1992b). The cell pellet was lysed in pH 9.0 buffer, and $cPLA_2$ in the supernatant was precipitated with $(NH_4)_2SO_4$ (30%–45%). Heparin sepharose, Q sepharose, and size exclusion chromatography steps yielded protein samples suitable for crystallization experiments. Analysis by capillary electrophoresis indicated that the protein was heterogeneously phosphorylated. A typical yield from a 100 g pellet was 15–25 mg of pure $cPLA_2$ (M. Stahl et al., unpublished data).

Crystals of $cPLA_2$ were obtained by vapor diffusion at 18°C using 0.1 M MES (pH 6.2), 30 mM spermidine, 8% PEG 1000, 13% DMSO, and 12 mg/ml protein. Typically, plate-like crystals appeared overnight and continued to grow to a maximum size of 0.6 mm × 0.5 mm × 0.1 mm within 1 week. Native and heavy atom–soaked crystals were cryoprotected by transferring into increasing amounts of PEG 400 and DMSO. Heavy atom–modified crystals were prepared by soaking native crystals overnight in cryosolution with $CaCl_2$ replaced by 250 μM $TbCl_3$. Cryoprotected crystals were flash cooled in a gaseous nitrogen stream at 100 K prior to data collection.

Diffraction data of the native and Tb-soaked $cPLA_2$ crystals were collected at beamline 5.0.2 at the Advanced Light Source using a Quantum 4 CCD detector (Area Detector Systems). Due to crystal sensitivity, the first image of each data set was analyzed with STRATEGY (R. Ravelli; http://www.x12c.nsls.bnl.gov/x12c/man_strategy/man_strategy2.html) in an effort to calculate the minimum amount of data collection required for a complete data set. After the determination of the optimal starting point, data were collected through a 90° sweep, after which the crystals were rotated to a position 180° from the starting point and a second 90° sweep was collected with a view toward maximizing Bijvoet pair accumulation. Crystals started displaying radiation sensitivity after approximately 100° of data collection, making it necessary to translate them along the rotation axis between wavelength changes. This methodology proved to be successful in that data sets collected from three different wavelengths displayed similar statistics. All data were collected at 100 K and processed with DENZO/SCALEPACK (Otwinowski, 1993).

### Heavy Atom Sites

Both Tb sites were identified by visual inspection of anomalous Patterson maps using diffraction data collected at the peak wavelength of the Tb $L_{III}$ edge (see Table 1), confirming results from previous lower resolution Tb data sets collected on an in-house Raxis IV detector (Molecular Structure Corp.). Heavy atom parameter refinement and phasing were accomplished with SHARP (de la Fortelle and Bricogne, 1997). Density modification was performed in SOLOMON (CCP4, 1994) as implemented in SHARP. The high quality experimental 3.2 Å electron density map allowed for the positioning of the entire C2 domain as well as the initial tracing and sequence assignment of the catalytic domain (Quanta); this procedure facilitated the calculation of a mask encompassing the protein region, which was included in further calculations. These included histogram matching, two-fold noncrystallographic symmetry averaging, and phase extension from 3.2 to 2.5 Å using the native diffraction data in DM (Cowtan and Main, 1996). Cycles of phase combination and refinement were performed with REFMAC (Murshudov et al., 1997), generating a map in which most of the model could be identified, including central residues of the flexible lid.

### Refinement

Cycles of rebuilding as well as positional and thermal parameter refinement in XPLOR (Brünger, 1992b) were used to improve the model, which was submitted to simulated annealing refinement (Brünger et al., 1990) (12–2.5 Å) after the $R_{free}$ had dropped below 32% (Brünger, 1992a). Subsequent model-building stages were performed with the aid of omit maps generated through maximum-likelihood refinement as implemented in BUSTER (Bricogne, 1993). Refinement also included a uniform bulk solvent correction (Bsol = 23.8 $Å^2$; ksol = 0.305 $e^-/Å^3$) and the application of noncrystallographic symmetric restraints. All diffraction data with $F > 2.0$ (88.6% of all reflections) were used throughout the refinement except for a 10% randomly selected test set, which was used for calculation of $R_{free}$. Fo-Fc maps were used to locate water molecules, which were placed at sites that displayed densities $>3.0\sigma$ and exhibited reasonable protein–solvent hydrogen bonding distances without steric conflict. The final model contains 1260 residues (molecule A: 13–433, 457–498, and 540–721) and 48 water molecules; it exhibits good stereochemistry, with an average bond length and bond angle deviation from ideal geometry of 0.016 Å and 1.94°, respectively. 98.1% of all residues are in most favorable and additionally allowed regions of a Ramachandran plot, with 0.4% in disallowed regions. The overall free R value is 29.8%, and the R factor is 22.9% using diffraction data between 12 and 2.5 Å (Table 1).

## Acknowledgments

We thank S. Venuti and R. Zollner for a tireless effort in CHO cell growth, as well as P. Towler, A. Boodhoo, and T. Noland for assistance with protein purification. We are grateful to Thomas Earnest and the Advanced Light Source 5.0.2. Beamline group for assistance with data collection. We are indebted to John Knopf for his continuing support.

Received February 18, 1999; revised March 31, 1999.

## References

Altschul, S.F., Madden, T.L., Schäffer, A.A., Zhang, J., Zhang, Z., Miller, W., and Lipman, D.J. (1997). Gapped BLAST and PSI-BLAST: a new generation of protein database search programs. Nucleic Acids Res. *25*, 3389–3402.

Bacon, D.J., and Anderson, W.F. (1988). A fast algorithm for rendering space-filling molecule pictures. J. Mol. Graph. *6*, 219–220.

Bonventre, J.V., Huang, Z., Reza Taheri, M., O'Leary, E., Li, E., Moskowitz, M.A., and Sapirstein, A. (1997). Reduced fertility and postischaemic brain injury in mice deficient in cytosolic phospholipase $A_2$. Nature *390*, 622–625.

Börsch-Haubold, A.G., Bartoli, F., Asselin, J., Dudler, T., Kramer, R.M., Apitz-Castro, R., Watson, S.P., and Gelb, M.H. (1998). Identification of the phosphorylation sites of cytosolic phospholipase $A_2$ in agonist-stimulated human platelets and HeLa cells. J. Biol. Chem. *273*, 4449–4458.

Bricogne, G. (1993). Direct phase determination by entropy maximization and likelihood ranking: status report and perspectives. Acta Crystallogr. *D49*, 37–60.

Brünger, A.T. (1992a). The free R value: a novel statistical quantity for assessing the accuracy of crystal structures. Nature *355*, 472–474.

Brünger, A.T. (1992b). X-PLOR version 3.1. A system for x-ray crystallography and NMR (New Haven: Yale University Press).

Brünger, A.T., Krukowski, A., and Erickson J. (1990). Slow-cooling protocols for crystallographic refinement by simulated annealing. Acta Crystallogr. *A46*, 585–593.

CCP4 (1994). The CCP4 suite: programs for X-ray crystallography. Acta Crystallogr. *D50*, 760–763.

Clark, J.D., Lin, L.-L., Kriz, R.W., Ramesha, C.S., Sultzman, L.A., Lin, A.Y., Milona, N., and Knopf, J.L. (1991). A novel arachidonic acid-selective cytosolic $PLA_2$ contains a $Ca^{2+}$-dependent translocation domain with homology to PKC and GAP. Cell *65*, 1043–1051.

Clark, J.D., Schievella, A.R., Nalefski, E.A., and Lin, L.-L. (1995). Cytosolic phospholipase $A_2$. J. Lipid Mediat. Cell Signal. *12*, 83–117.

Cleland, W.W., and Kreevoy, M.M. (1994). Low-barrier hydrogen bonds and enzymic catalysis. Science *264*, 1887–1890.

Cowtan, K.D., and Main, P. (1996). Phase combination and cross

validation in iterated density modification calculations. Acta Crystallogr. *D42*, 43–48.

Cygler, M., and Schrag, J.D. (1997). Structure as basis for understanding interfacial properties of lipases. Meth. Enzymol. *284*, 3–27.

de Carvalho, M.G.S., McCormack, A.L., Olson, E., Ghomaschi, F., Gelb, M., Yates, J.R., III, and Leslie, C.C. (1996). Identification of phosphorylation sites of human 85 kDa cytosolic phospholipase $A_2$ expressed in insect cells and present in human monocytes. J. Biol. Chem. *271*, 1–11.

de la Fortelle, E., and Bricogne, G. (1997). Maximum-likelihood heavy-atom parameter refinement for multiple isomorphous replacement and multiwavelength anomalous diffraction methods. Methods Enzymol. *276*, 494–523.

Dennis, E.A. (1997). The growing phospholipase $A_2$ superfamily of signal transduction enzymes. Trends Biochem. Sci. *22*, 1–2.

Derewenda, Z.S, and Derewenda, U. (1991). Relationships among serine hydrolases: evidence for a common structural motif in triacylglyceride lipases and esterases. Biochem. Cell. Biol. *69*, 842–851.

Duggleby, H.J., Tolley, S.P., Hill, C.P., Dodson, E.J., Dodson, G., and Moody, P.C.E. (1995). Penicillin acylase has a single-amino-acid catalytic centre. Nature *373*, 264–268.

Essen, L.-O., Perisic, O., Cheung, R., Katan, M., and Williams, R.L. (1996). Crystal structure of a mammalian phosphoinositide-specific phospholipase Cδ. Nature *380*, 595–602.

Glover, S., de Carvalho, M., Bayburt, T., Jonas, M., Chi, E., Leslie, E., and Gelb, M. (1995). Translocation of the 85-kDa phospholipase $A_2$ from cytosol to the nuclear envelope in rat basophilic leukemia cells stimulated with calcium ionophore or IgE/antigen. J. Biol. Chem. *270*, 15359–15367.

Grobler, J.A., Essen, L.-O., Williams, R.L., and Hurley, J.H. (1996). C2 domain conformational changes in phospholipase Cδ1. Nat. Struct. Biol. *3*, 788–795.

Hanel, A.M., and Gelb, M.H. (1993). Processive interfacial catalysis by mammalian 85-kilodalton phospholipase $A_2$ enzymes on product-containing vesicles: application to the determination of substrate preferences. Biochemistry *32*, 5949–5958.

Hanel, A.M., and Gelb, M.H. (1995). Multiple enzymatic activities of the human cytosolic 85-kDa phospholipase $A_2$: hydrolytic reactions and acyl transfer to glycerol. Biochemistry *34*, 7807–7818.

Hendrickson, W.A. (1991). Determination of macromolecular structures from anomalous diffraction of synchrotron radiation. Science *254*, 51–58.

Hixon, M.S., Ball, A., and Gelb, M.H. (1998). Calcium-dependent and -independent interfacial binding and catalysis of cytosolic group IV phospholipase $A_2$. Biochemistry *37*, 8516–8526.

Huang, Z., Payette, P., Abdullah, K., Cromlish, W.A., and Kennedy, B.P. (1996). Functional identification of the active-site nucleophile of the human 85-kDa cytosolic phospholipase $A_2$. Biochemistry *35*, 3712–3721.

Kraulis, P.J. (1991). MOLSCRIPT: a program to produce both detailed and schematic plots of protein structures. J. Appl. Crystallogr. *24*, 946–950.

Leslie, C.C. (1997). Properties and regulation of cytosolic phospholipase $A_2$. J. Biol. Chem. *272*, 16709–16712.

Leslie, C.C., and Channon, J.Y. (1990). Anionic phospholipids stimulate an arachidonoyl-hydrolyzing phospholipase $A_2$ from macrophages and reduce the calcium requirement for activity. Biochim. Biophys. Acta *1045*, 261–270.

Lin, L.-L., Lin, A.Y., and DeWitt, D.L. (1992a). IL-1 a induces the accumulation of cPLA$_2$ and the release of PGE2 in human fibroblasts. J. Biol. Chem. *267*, 23451–23454.

Lin, L.-L., Lin, A.Y., and Knopf, J.L. (1992b). Cytosolic phospholipase $A_2$ is coupled to hormonally regulated release of arachidonic acid. Proc. Natl. Acad. Sci. USA *89*, 6147–6151.

Lin, L.-L., Wartmann, M., Lin, A.Y., Knopf, J.L., Seth, A., and Davis, R.J. (1993). cPLA$_2$ is phosphorylated and activated by MAP kinase. Cell *72*, 269–278.

Matagne, A., Lamotte-Brasseur, J., and Frère, J.-M. (1998). Catalytic properties of class A β-lactamases: efficiency and diversity. Biochem. J. *330*, 581–598.

Mosior, M., Six, D.A., and Dennis, E.A. (1998). Group IV cytosolic phospholipase $A_2$ binds with high affinity and specificity to phosphatidylinositol 4,5-bisphosphate resulting in dramatic increases in activity. J. Biol. Chem. *273*, 2184–2191.

Murshudov, G.N., Vagin, A.A., and Dodson, E.J. (1997). Acta Crystallogr. Sect. D. *53*, 240–255.

Nalefski, E.A., and Falke, J.J. (1996). The C2 domain calcium-binding motif: structural and functional diversity. Protein Sci. *12*, 2375–2390.

Nalefski, E.A., and Falke, J.J. (1998). Location of the membrane-docking face on the $Ca^{2+}$-activated C2 domain of cytosolic phospholipase $A_2$. Biochemistry *37*, 17642–17650.

Nalefski, E.A., Sultzman, L.A., Martin, D.M., Kriz, R.W., Towler, P.S., Knopf, J.L., and Clark, J.D. (1994). Delineation of two functionally distinct domains of cytosolic phospholipase $A_2$, a regulatory $Ca^{2+}$-dependent lipid-binding domain and a $Ca^{2+}$-independent catalytic domain. J. Biol. Chem. *269*, 18239–18249.

Nalefski, E.A., McDonagh, T., Somers, W. , Seehra, J., Falke, J.J., and Clark, J.D. (1998). Independent folding and ligand specificity of the C2 calcium-dependent lipid binding domain of cytosolic phospholipase $A_2$. J. Biol. Chem. *273*, 1365–1372.

Nicholls, A. (1992). GRASP: graphical representation and analysis of surface properties (Columbia University, NY).

O'Byrne, P.M. (1997). Leukotrienes in the pathogenesis of asthma. Chest *111*, 27S–34S.

Otwinowski, Z. (1993). In Data Collection and Processing. L. Sawyer, N. Isaacs, and S.W. Bailey, eds. (Daresbury, U.K.: Science and Engineering Council), pp. 56–62.

Perisic, O., Fong, S., Lynch, D.E., Bycroft, M., and Williams, R.L. (1998). Crystal structure of a calcium-phospholipid binding domain from cytosolic phospholipase $A_2$. J. Biol. Chem. *273*, 1596–1604.

Pickard, R.T., Chiou, X.G., Strifler, B.A., DeFelippis, M.R., Hyslop, P.A., Tebbe, A.L., Yee, Y.K., Reynolds, L.J., Dennis, E.A., Kramer, R.M., and Sharp, J.D. (1996). Identification of essential residues for the catalytic function of 85-kDa cytosolic phospholipase $A_2$. J. Biol. Chem. *271*, 19225–19231.

Qiu, Z.-H., Gijón, M.A., de Carvalho, M.S., Spencer, D.M., and Leslie, C.C. (1998). The role of calcium and phosphorylation of cytosolic phospholipase $A_2$ in regulating arachidonic acid release in macrophages. J. Biol. Chem. *273*, 8203–8211.

Rao, V.D., Misra, S., Boronekov, I.V., Anderson, R.A., and Hurley, J.H. (1998). Structure of type IIβ phosphatidylinositol phosphate kinase: a protein kinase fold flattened for interfacial phosphorylation. Cell *94*, 829–839.

Reynolds, L.J., Hughes, L.L., Louis, A.I., Kramer, R.M., and Dennis, E.A. (1993). Metal ion and salt effects on the phospholipase $A_2$, lysophospholipase, and transacylase activities of human cytosolic phospholipase $A_2$. Biochim. Biophys. Acta *1167*, 272–280.

Schievella, A.R., Regier, M.K., Smith, W.L., and Lin, L.-L. (1995). Calcium-mediated translocation of cytosolic phospholipase $A_2$ to the nuclear envelope and endoplasmic reticulum. J. Biol. Chem. *270*, 30749–30754.

Schrag, J.D., and Cygler, M. (1997). Lipases and α/β hydrolase fold. Meth. Enzymol. *284*, 85–107.

Scott, D.L., White, S.P., Zbyszed, O., Yan, W., Gelb, M.H., and Sigler, P.B. (1990). Interfacial catalysis: the mechanism of phospholipase $A_2$. Science *250*, 1541–1546.

Sharp, J.D., Pickard, R.T., Chiou, X.G., Manetta, J.V., Kovacevic, S., Miller, J.R., Varshavsky, A.D., Roberts, E.F., Strifler, B.A., Brems, D.N., et al. (1994). Serine 228 is essential for catalytic activities of 85-kDa cytosolic phospholipase $A_2$. J. Biol. Chem. *269*, 23250–23254.

Simon, L.S., Lanza, F.L., Lipsky, P.E., Hubbard, R.C., Talwalker, S., Schwartz, B.D., Isakson, P.C., and Geis, G.S. (1998). Preliminary study of the safety and efficacy of SC-58635, a novel cyclooxygenase 2 inhibitor: efficacy and safety in two placebo-controlled trials in osteoarthritis and rheumatoid arthritis, and studies of gastrointestinal and platelet effects. Arthritis Rheum. *41*, 1591–1602.

Tjoelker, L.W., Wilder, C., Eberhardt, C., Stafforini, D.M., Dietsch, G., Schimpf, B., Hooper, S., Le Trong, H., Cousens, L.S., Zimmerman, G.A., et al. (1995). Anti-inflammatory properties of a platelet-activating factor acetylhydrolase. Nature *374*, 549–553.

Trimble, L.A., Street, I.P., Perrier, H., Tremblay, N.M., Weech, P.K., and Bernstein, M.A. (1993). NMR structural studies of the tight complex between a trifluoromethyl ketone inhibitor and the 85-kDa human phospholipase $A_2$. Biochemistry *32*, 12560–12565.

Underwood, K.W., Song, C., Kriz, R.W., Chang, X.J., Knopf, J.L., and Lin, L.-L. (1998). A novel calcium-independent phospholipase $A_2$, cPLA$_2$-γ, that is prenylated and contains homology to cPLA$_2$. J. Biol. Chem. *273*, 21926–21932.

Uozumi, N., Kume, K., Nagase, T., Nakatani, N., Ishii, S., Tashiro, F., Komagata, Y., Maki, K., Ikuta, K., Ouchi, Y., Miyazaki, J-i., and Shimizu, T. (1997). Role of cytosolic phospholipase $A_2$ in allergic response and parturition. Nature *390*, 618–622.

Venable, M.E., Olson, S.C., Nieto, M.L., and Wykle, R.L. (1993). Enzymatic studies of lyso platelet-activating factor acylation in human neutrophils and changes upon stimulation. J. Biol. Chem. *268*, 7965–7975.

Xu, G.-Y., McDonagh, T., Yu, H.-A., Nalefski, E., Clark, J.D., and Cumming, D.A. (1998). Solution structure and membrane interactions of the C2 domain of cytosolic phospholipase $A_2$. J. Mol. Biol. *280*, 485–500.

**Protein Data Bank ID Code**

The ID code for human cPLA$_2$ is 1cjy.